Rapid bench-top fabrication of poly(dimethylsiloxane)/polystyrene microfluidic devices incorporating high-surface-area sensing electrodes

Sanjay Sonney, Norman Shek, and Jose M. Moran-Mirabal[a)]
Department of Chemistry and Chemical Biology, McMaster University, Hamilton, Ontario L8S 4M1, Canada

(Received 26 January 2015; accepted 7 April 2015; published online 13 April 2015)

The development of widely applicable point-of-care sensing and diagnostic devices can benefit from simple and inexpensive fabrication techniques that expedite the design, testing, and implementation of lab-on-a-chip devices. In particular, electrodes integrated within microfluidic devices enable the use of electrochemical techniques for the label-free detection of relevant analytes. This work presents a novel, simple, and cost-effective bench-top approach for the integration of high surface area three-dimensional structured electrodes fabricated on polystyrene (PS) within poly(dimethylsiloxane) (PDMS)-based microfluidics. Optimization of PS-PDMS bonding results in integrated devices that perform well under pressure and fluidic flow stress. Furthermore, the fabrication and bonding processes are shown to have no effect on sensing electrode performance. Finally, the on-chip sensing capabilities of a three-electrode electrochemical cell are demonstrated with a model redox compound, where the high surface area structured electrodes exhibit ultra-high sensitivity. We propose that the developed approach can significantly expedite and reduce the cost of fabrication of sensing devices where arrays of functionalized electrodes can be used for point-of-care analysis and diagnostics.

[http://dx.doi.org/10.1063/1.4918596]

I. INTRODUCTION

The development of lab-on-a-chip (LoC) platforms for point-of-care detection and diagnostics requires the integration of sensing and transduction elements within fluidic channels of sub-millimetre dimensions. In particular, the encapsulation of electrodes within microfluidic channels enables the on-chip use of electrochemical sensing techniques that provide highly sensitive detection of label-free analytes over a wide range of concentrations.[1–3] To date, most microelectrodes integrated into LoC devices have been mostly fabricated using techniques inherited from the semiconductor industry (e.g., photolithography, thin film deposition, etching, and anodic bonding).[4] Despite the success of these techniques in producing fully assembled devices, they typically entail the use of one or more costly and time-consuming processes that require access to clean-room facilities. Inexpensive benchtop photolithography has been successfully used to expedite the development of microfabricated devices without clean-room facilities.[5] Yet, these approaches still rely on multi-step, lengthy and laborious processes and do not allow direct patterning of thin films or the formation of three-dimensional (3D) structured surfaces. These constraints still hinder the rapid development of inexpensive point-of-care devices that can be deployed in a variety of applications.

[a)]Author to whom correspondence should be addressed. Electronic mail: mirabj@mcmaster.ca

To overcome these limitations, non-traditional bench-top fabrication methods have been developed to prototype and fabricate micro- and nanostructured materials.[4] These approaches include techniques such as razor-blade cutting (xurography),[6,7] adhesive film masking,[8] and structuring through shape-memory polymers (SMPs),[9,10] among many others. Using these techniques, it has been possible to prototype microfluidic channels,[11–13] pattern thin films and surfaces,[8,14] and produce micro and nanostructured metallic surfaces[15–17] that have been applied mostly to Surface Enhanced Raman Scattering (SERS) applications.[18–20] The simplicity and cost-effectiveness of bench-top fabrication methods make them ideal for prototyping, optimizing, and producing low-cost disposable LoC devices.

Recently, heat-shrinkable SMPs have been used as inexpensive and convenient materials for the bench-top fabrication of structured surfaces. Some of the uses for these materials include reducing the size of microfluidic channels and patterned surfaces,[21,22] and structuring thin films through compressive stress.[16,23,24] Our group[15,25] and others[20,26,27] have used the latter approach to structure gold films with features that are tuneable in the micro- to nanoscale. The structured gold films, when used as SERS substrates[20] or as working electrodes in an electrochemical setup,[15] present enhanced surface area that can significantly improve sensitivity. Thus, this simple bench-top fabrication approach could be applied to developing high surface area electrodes for sensing within LoC devices.

This manuscript presents for the first time a simple, rapid, and cost-effective bench-top method for the integration of high surface area 3D-structured electrodes into LoC devices. Polystyrene (PS) and poly(dimethylsiloxane) (PDMS) were used as substrates for the fabrication of structured electrodes and microfluidic channels, respectively. The two substrates were bonded through plasma oxidation and an intermediate silane layer. The bonding conditions were optimized, and the bonded LoC devices were stress-tested. Using cyclic voltammetry, the electro-active surface area (ESA) of the electrodes was measured throughout fabrication to assess the impact of different treatments on electrode functionality. A three-electrode electrochemical cell was implemented on-chip with a salt-bridge-free structured platinum reference electrode and was used to demonstrate the sensing capabilities of the bench-top fabricated devices. It is anticipated that the methods presented will aid in the development of inexpensive and disposable point-of-care sensing and diagnostic devices.

II. MATERIALS AND METHODS

A. Preparation of structured electrode layer

Thin (50–200 nm) metallic films were patterned and 3D structured on PS substrates as previously described.[15] Briefly, PS substrates (Grafix Shrink Film, Graphix, Maple Heights, OH) were cut to the desired shapes and cleaned by washing in successive isopropyl alcohol, ethanol, and water baths under continuous agitation at 50 rpm and dried under a nitrogen stream. Self-adhesive vinyl (FDC-4300, FDC graphics films, South Bend, IN) sheets were patterned using a blade cutter (Graphtec ROBO Pro CE5000-40-CRP, Graphtec America, Inc., Irvine, CA) and adhered onto the clean PS substrates to serve as sputtering masks. Gold or platinum was sputtered onto the masked PS substrates at a rate of $\sim$1 Å/s using a Torr Compact Research Coater CRC-600 manual planar magnetron sputtering system (New Windsor, NY). The vinyl mask was removed after sputtering, and the PS substrate was heated to 160 °C to shrink the device and structure the patterned metallic films. Nalgene (Penfield, NY) PVC 1/32 in. inner, 3/32 in. outer diameter tubing was used at the inlet/outlet fluidic ports. The PS substrate was designed with inlet/outlet holes that shrink to form a tight seal with the tubing. One end of the tubing was sharpened with a razor and threaded through the hole until the tubing no longer protruded from the PS substrate, leaving a flat surface for bonding. To seal the tubing in place, optical adhesive 88 (Norland Products, Inc., Cranbury, NJ) was applied on the non-bonding face of the PS and cured for 20 min in an UV illumination chamber. Two electrode designs were prepared; one to characterize electro-active surface area (device 1) and the other, based on a design previously described by Dydek *et al.*,[3] was used for electrochemical sensing (device 2). All electrodes in device 1, as well as the working and counter electrodes in device 2, were made from

50 nm-thick gold films, while the reference electrodes in device 2 were made from 50 nm-thick platinum films.

B. Fabrication of microfluidic channel layer

Clear scotch tape (3M, St. Paul, MN) was used to prepare moulds for the microfluidic layers. The tape was applied to a transparency sheet and patterned with a blade cutter. The excess tape was peeled off from the transparency, and the patterned motifs were used as negative moulds for the fabrication of microfluidic layers. The sheets containing the moulds were adhered onto a plastic dish, and 8:1 (v/v) elastomer to hardener PDMS mix (Sylgard 184, Dow Corning, Midland, MI) was cast and cured for 24 h at room temperature. Immediately before bonding, the microfluidic layers were manually cut out of the petri dish with a razor blade and treated with oxygen plasma for 30 s (30 sccm air inlet flow, 600 mTorr) at high power setting (30 W) in a PDC expanded plasma cleaner (Harrick, Ithaca, NY).

C. Bonding of structured electrode and microfluidic layers

The PS and PDMS layers were bonded using (3-Aminopropyl)triethoxysilane (APTES, Sigma-Aldrich, Oakville, ON) as an intermediate bonding layer. First, the shrunken PS surface was oxidized in a PDC expanded plasma cleaner (30 sccm air inlet flow, 600 mTorr) at high power setting (30 W). Then it was immersed in an APTES solution in 18.2 MΩ water at 80 °C for 20 min, and subsequently dried with a nitrogen stream. Finally, the PDMS layer was aligned and pressed onto the PS layer to ensure a tight seal. The devices were allowed to cure at room temperature and in some cases were heat treated to promote the formation of a strong bond.

D. Characterization of bond strength

The failure pressure was measured in devices with a $7 \times 7 \times 0.04$ mm dead-end chamber as previously described by Eddings *et al.*[28] A 5.8 mm frame around the chamber, with a bonding area of 300 mm^2, was used to seal the chamber. The devices were attached to a pressurized nitrogen gas line and immersed in water. The pressure was increased gradually until the device failed and vigorous gas bubbling was observed. This was recorded as the failure pressure. Devices with the same dimensions but with glass instead of polystyrene were prepared and tested as a reference point for the glass-PDMS bond strength. Similarly, the failure flow rate of bonded devices was assessed with a PHD ULTRA^{TM} Syringe Pump (Harvard Apparatus, Holliston, MA). A microfluidic test device was constructed with a straight channel, 6 mm in length, 150 μm in width, and 40 μm in height. A 1 mM solution of Rhodamine B in 18.2 MΩ water was used to visualize the channel and check for bond failure. The pump was programmed to deliver increasing flow rates from 0.1 ml/min to 10 ml/min and the rate at which the device failed was recorded.

E. Characterization of the electro active surface area

The ESA of the working electrodes in device 1 was assessed throughout the device fabrication process. Changes in the electrode performance were assessed by monitoring the formation of a monolayer of gold oxide on the surface of the devices through cyclic voltammetry using a CH Instruments 600E electrochemical workstation (Austin, TX). The gold working electrode was immersed in 50 mM H_2SO_4 solution, and 10 scans were performed from 0 to 1.5 V (relative to an external Ag/AgCl electrode) at a rate of 0.1 V s^{-1}. The reduction peak in the resulting chromatograms was then integrated to determine the total charge required to reduce the working electrode, which was used as the nominal ESA.

F. Electrochemical detection within microfluidic devices

$K_4[Fe(CN)_6]$ solutions from 10 nM to 140 mM were prepared in 1 M KCl background electrolyte solution. A calibration curve was generated using device 2 through chronoamperometry using a CH Instruments 600E electrochemical workstation (Austin, TX) at a potential of 0.3 V

relative to the on-chip platinum structured electrode. The current measured 1 s after applying the potential was recorded for each $K_4[Fe(CN)_6]$ concentration.

III. RESULTS AND DISCUSSION

A. Device layer fabrication through bench-top techniques

The use of a blade cutter (xurography) allowed the rapid prototyping and fabrication of both the structured electrode and microfluidic layers (Fig. 1). In the electrode layer, xurography was used to cut 6 mm fluidic inlet and outlet holes directly into the PS substrate, as well as to cut a vinyl electrode mask that was adhered to the PS substrate to define the shape and dimensions of the patterned electrodes. The smallest feature size that could be obtained reproducibly in the vinyl mask was 100 μm, which is limited by the cutter step size. Sputtering a 50 nm-thick gold film and lifting the vinyl mask off revealed the patterned electrodes. The PS substrate containing the patterned electrodes was then heated above the glass transition temperature of polystyrene ($\sim$100 °C) to homogeneously shrink the electrode layer to $\sim$16% of its original area. Each transverse dimension of the device shrunk to 37.5% $\pm$ 0 .6% (n = 7) of the original size highlighting the high reproducibility of the fabrication through shape-memory polymer approach. The compressive stress from the shrinking process caused the electrodes to wrinkle (cf. Fig. 3), resulting in a $\sim$6-fold increase in Au electrode surface per geometrical surface area. Scanning electron microscopy images revealed no visible tears or defects in the metallic films either before or after the shrinking process, and no spontaneous delamination of the electrode layers was observed during shrinking or during repeated (5×) adhesion and peeling of an adhesive tape. The topography of the resulting 3D structured gold films had a root mean square surface roughness of 560 $\pm$ 10 nm as measured through optical profilometry (Fig. S1 in the supplementary material[30]). Shrinking the PS substrate also had the effect of reducing the diameter of the fluidic inlet and outlet holes to 2.4 mm, which was slightly smaller than the outer diameter of the tubing used. Threading the tubing through the inlet/outlet holes and sealing with UV-curable adhesive provided robust fluidic connections that did not fail under the pressurization and flow conditions tested.

PDMS layers were also quickly and inexpensively fabricated using xurography (Fig. 1). Microfluidic layers were fabricated by cutting the negative moulds from tape, casting PDMS, and curing overnight. The resulting layers were cut out manually from the cured PDMS and contained microfluidic channels and chambers with a depth of 40 μm, corresponding to the tape thickness. Features cut into the clear tape, down to 100 μm feature size, were faithfully reproduced in the microfluidic layers. This procedure allowed us to easily prototype and test microfluidic channel layouts that went from simple straight channels to complex fluidic chambers (Fig. S2 in the supplementary material[30]).

B. Bonding of structured electrode and microfluidic layers

Complete bench-top-fabricated microfluidic channels were assembled by bonding the structured electrode and microfluidic layers. Successful bonding was achieved through a process consisting of: (i) air plasma oxidation of the PS substrate followed by APTES treatment, (ii) air plasma oxidation of the PDMS layer, and (iii) pressing together the treated layers and allowing the bond to cure. To study the effects of bonding parameters on bond strength, the PS substrate plasma treatment time, APTES concentration, and thermal treatment after bonding were independently varied, while keeping the air plasma oxidation time of the PDMS microfluidic layer constant.

The bond strength for assembled devices was assessed using two microfluidic chip designs. A dead-end chamber design was used to measure the pressure at which the device burst or delaminated, while a straight channel was used to measure the flow rate that caused the device to fail. It was observed that both plasma oxidation and APTES treatment of the PS layer were necessary to form a strong bond between the microfluidic and electrode layers, as the omission of either led to significantly lower failure pressure and flow rates (at 99% confidence, Figs. 2(a) and 2(b)). No

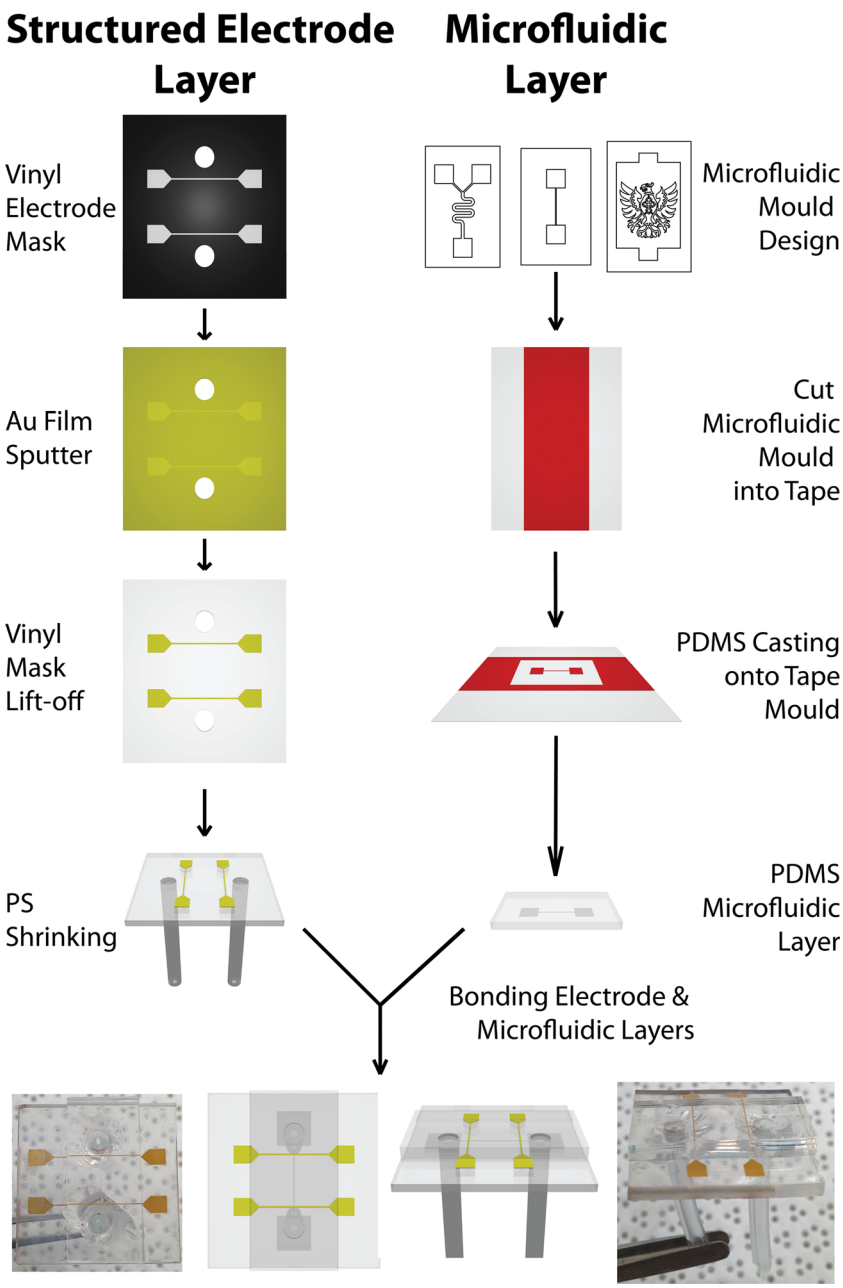

FIG. 1. Schematic of the bench-top fabrication techniques used to integrate 3D structured electrodes within microfluidic channels. Structured electrode layer fabrication (left): Electrodes are patterned by attaching a pre-cut vinyl electrode mask (black) to a pre-stressed PS substrate, sputtering a thin gold film (yellow) and lifting the mask off. Heating the PS substrate causes it to shrink and structures the gold film. Unshrunken electrode layer is not drawn to scale. Microfluidic layer fabrication (right): Negative moulds are prepared by patterning adhesive tape (red) on a carrier sheet. PDMS is cast over the negative mould and cured to create the microfluidic layer. The structured electrode and microfluidic layers are bonded through oxygen plasma and APTES treatment to form the complete microfluidic system. Insets show two views of actual completed devices encapsulating two straight structured electrodes spanning a 100 μm wide microfluidic channel.

statistical difference in failure pressure was observed for devices where the PS substrates were plasma oxidized for 30, 60, or 90 s and subsequently treated with 5% APTES (Fig. 2(a)). However, significant differences (at 95% confidence) were observed for the failure flow rates of straight channel devices prepared under the same conditions, with 60 s plasma oxidation yielding the highest average failure flow rate (Fig. 2(a)). This result highlights the importance of testing the assembled devices under flow conditions, which cause the bond to respond differently than it

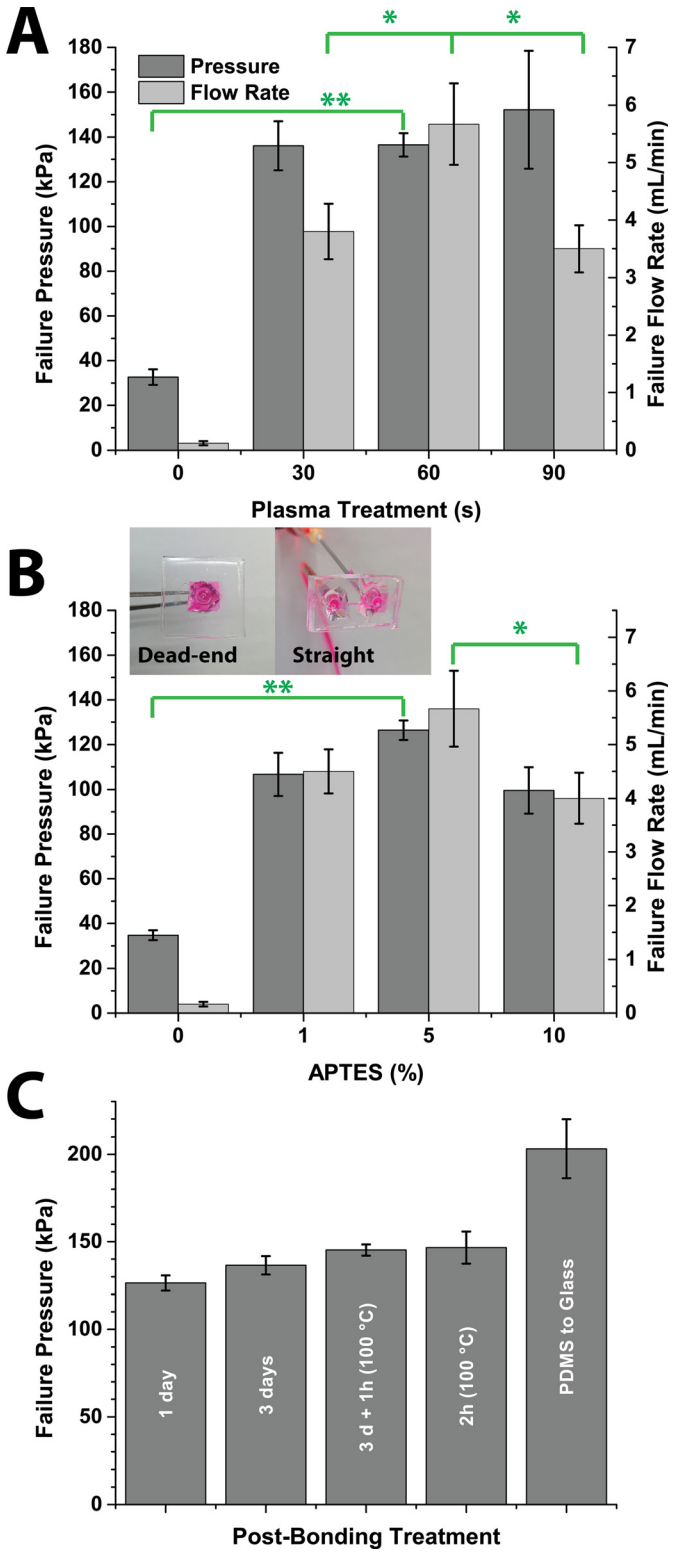

FIG. 2. Optimization of bonding conditions through failure pressure and failure flow rate tests. (a) Comparison of bond strength for PS substrates treated with varying plasma oxidation times followed by 5% APTES. (b) Comparison of PS substrates treated with 60 s plasma oxidation followed by treatment with varying APTES concentrations. (c) Effect of aging and thermal treatment on bond strength for PS substrates treated with 60 s plasma oxidation and 5% APTES. Insets: dead-end and straight channel devices used for measurements. Channels filled with coloured solution for visualization purposes. Statistical significance: **—at 99%, *—at 95% ($n > 3$).

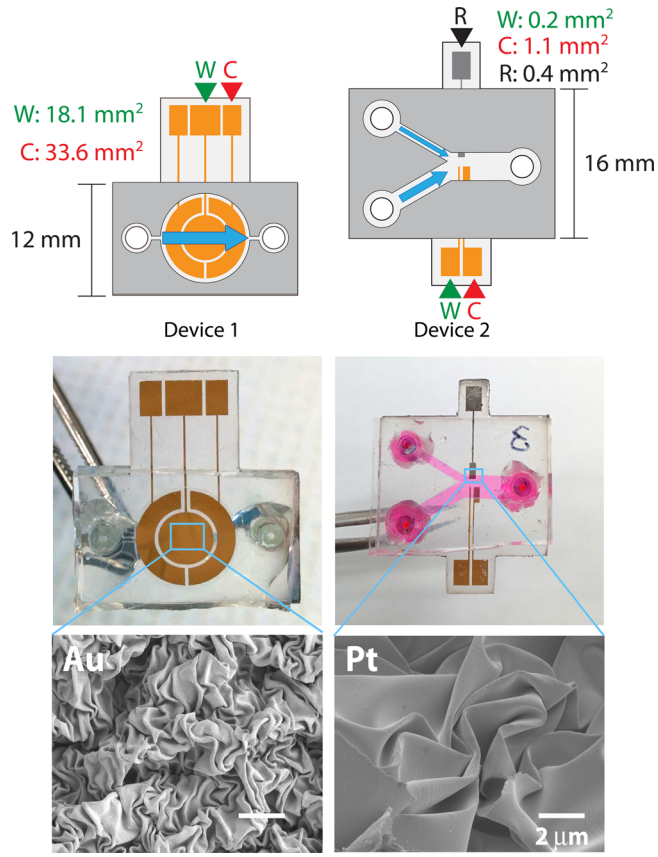

FIG. 3. Bench-top-fabricated layer designs used to integrate structured electrodes (light grey layer) within microfluidic channels (dark grey layer). Device 1 was designed with a central working electrode and two secondary electrodes that can be used as counter electrodes. Cyclic voltammetry was used with this device to quantify the electro-active surface area. Device 2 was used to perform electrochemical sensing of $K_4Fe(CN)_6$ in solution. Structured Au was used for the working and counter electrode, and structured Pt was used for the reference electrode.

does to evenly applied pressure, as in the dead-end chamber device. Likewise, the failure pressure and failure flow rate for devices assembled with PS substrates that underwent 60 s plasma oxidation followed by 1%, 5%, or 10% APTES treatment exhibited similar values (Fig. 2(b)), with the 5% APTES treatment displaying the highest average failure pressure (126 kPa) and average failure flow rate (5.67 ml/min). In light of these results, the protocol for bonding the structured electrode and microfluidic layers was settled at 60 s plasma oxidation of the PS substrate followed by 5% APTES treatment, and 30 s plasma oxidation of the PDMS layer. This protocol was used for all subsequently assembled devices.

The effect of ageing and thermal treatment on the bond strength was also tested in dead-end chamber devices. The bonded devices were tested after they had been aged for 1 and 3 days at room temperature, as well as aged for 3 days followed by thermal treatment for 1 h at 100 °C, and with no ageing followed by heating for 2 h at 100 °C (Fig. 2(c)). The bond strength showed slight improvement with ageing time at room temperature and through heating. With heating for 2 h at 100 °C after bonding, an average failure pressure of 147 kPa was measured which is ∼25% lower than the 203 kPa measured for PDMS-glass bonding. The fact that the strength of the bonds obtained with optimized conditions is reproducible and comparable to PDMS-glass bonds attests to the robustness of the developed bonding method.

C. Electrochemical sensing in microfluidic devices

Two electrode designs were prepared for electrochemical measurements with 3D structured electrodes encapsulated within bonded microfluidic devices (Fig. 3). Device 1 contained three

structured electrodes fabricated from 50 nm-thick gold films with circular or annular geometries that were used to assess the ESA. The ESA is a measure of the charge required to reduce/oxidize the gold electrode surface and, when measured comparatively through the fabrication process, can be used to assess the integrity of the electrode. Device 2 was used for electrochemical sensing and contained a three-electrode design, with working and counter structured electrodes fabricated from 50 nm-thick gold films and the reference electrode fabricated from 50 nm-thick platinum films. Both designs were bonded using the optimized protocol, and no adverse effect on bond strength was observed due to the presence of the structured electrodes.

The impact of the fabrication and bonding processes on the performance of structured gold electrodes was assessed by measuring the ESA through cyclic voltammetry (CV) in a mildly acidic solution. CV measurements were performed on three replicate devices at different points of the fabrication process: before shrinking, after shrinking, and after bonding in microfluidic channel (Fig. 4(a)). Integration of the cathodic peak in the resulting voltammograms yielded the total charge needed to reduce the surface of the gold electrode, which is proportional to its ESA. For direct comparisons, the measured values were normalized to the ESA of unshrunken electrodes (Fig. 4(b)). Despite the reduction of the electrode footprint to ∼1/6 of its original area and the increase in surface roughness, the ESA remained unchanged after shrinking. This indicated that the whole surface of the electrode was accessible and in contact with the acidic solution. Similarly, neither bonding nor encapsulation within the microfluidic channel significantly impacted the ESA and electrode performance. The integrity of the encapsulated electrodes was further evaluated by measuring the ESA on replicate devices with and without flow over 3 days after fabrication (Fig. 4(c)), where no significant change in ESA was observed over time. Altogether these results show that the 3D structured gold electrodes are not affected by the fabrication and bonding processes, and can be used to perform reproducible electrochemical measurements within microfluidics.

To perform on-chip electrochemical sensing, a salt-bridge-free three-electrode system was fabricated and encapsulated within a Y-shaped microfluidic channel. The design in device 2 takes advantage of the laminar flow within the microfluidic device to isolate the structured reference electrode without the need for a physical salt-bridge. Given that the potential of the platinum electrode depends on the concentration of hydronium ions, a buffer solution with constant pH was flowed over it to keep a constant potential. The other branch of the microfluidic device was used to flow solutions containing potassium ferricyanide at concentrations ranging from 10 nM to 140 mM over the working and counter electrodes. The redox active molecule was detected through chronoamperometry, and a calibration curve was constructed (Fig. 5). A positive correlation between concentration and anodic current was observed in the 1 μM–140 mM range, and excellent linearity was obtained in the 1–80 mM (Fig. 5(a)) and 10–1000 μM (Fig. 5(b)) ranges. These results highlight the capability to perform on-chip electrochemical sensing using bench-top fabricated 3D structured electrodes.

For the electrochemical sensing experiments, the lowest sensitivity was observed in the 1–80 mM range. Given that the total current, and thus the limit of detection of a microfluidic electrochemical sensor can be improved by making the electrode surface larger, an appropriate figure of merit for any sensing microelectrode is the sensitivity normalized per unit area. With a slope of 3.3 mA/M and taking into account the working electrode geometrical area of 0.2 mm^2, the calculated sensitivity per unit area for the on-chip electrochemical sensor is 1.65 ± 0.4 A/(M cm^2). To our knowledge, the sensitivity per unit area has only been reported for one other electrode, one based on vertically aligned carbon nanotubes, which exhibited a sensitivity per unit area of 0.0715 ± 0.0003 A/(M cm^2).[29] Thus, the sensitivity obtained with the 3D structured gold electrodes is ∼20 fold greater than the sensitivity achieved with vertically aligned carbon nanotube-based electrodes. The ultra-high sensitivity per unit area exhibited by the bench-top fabricated 3D structured electrodes is promising for on-chip biochemical sensing, an application our laboratory is currently pursuing through the selective functionalization of the 3D structured electrodes with targeted biorecognition elements.

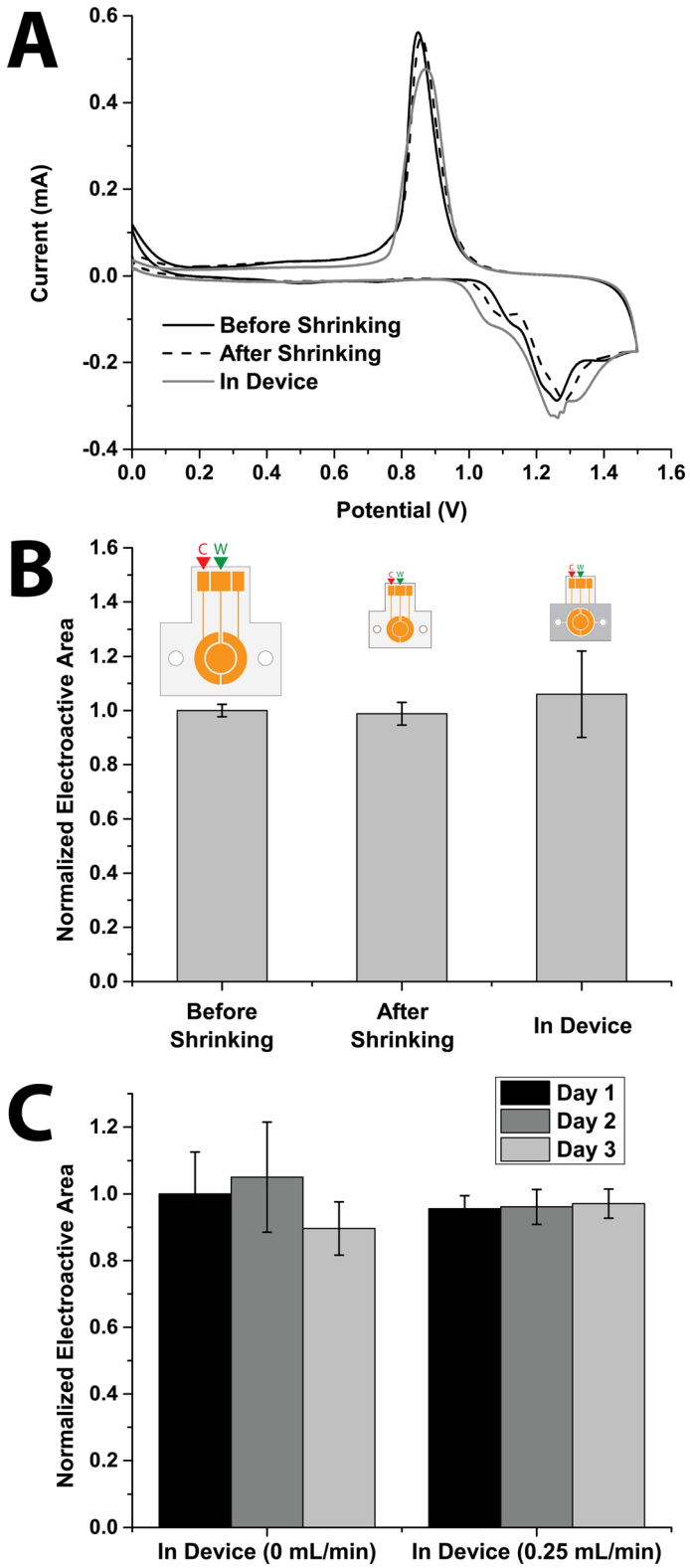

FIG. 4. Characterization of structured working electrode performance. (a) The ESA of structured gold electrodes was measured using cyclic voltammetry at different stages during the fabrication and encapsulation process. (b) The relative ESA remained unchanged, demonstrating that the fabrication, bonding, and enclosure in the microfluidic channel do not negatively affect the electrode integrity. (c) The reproducibility of ESA measurements was assessed over a three-day period. Error bars represent the standard deviation of measurements from three replicate devices.

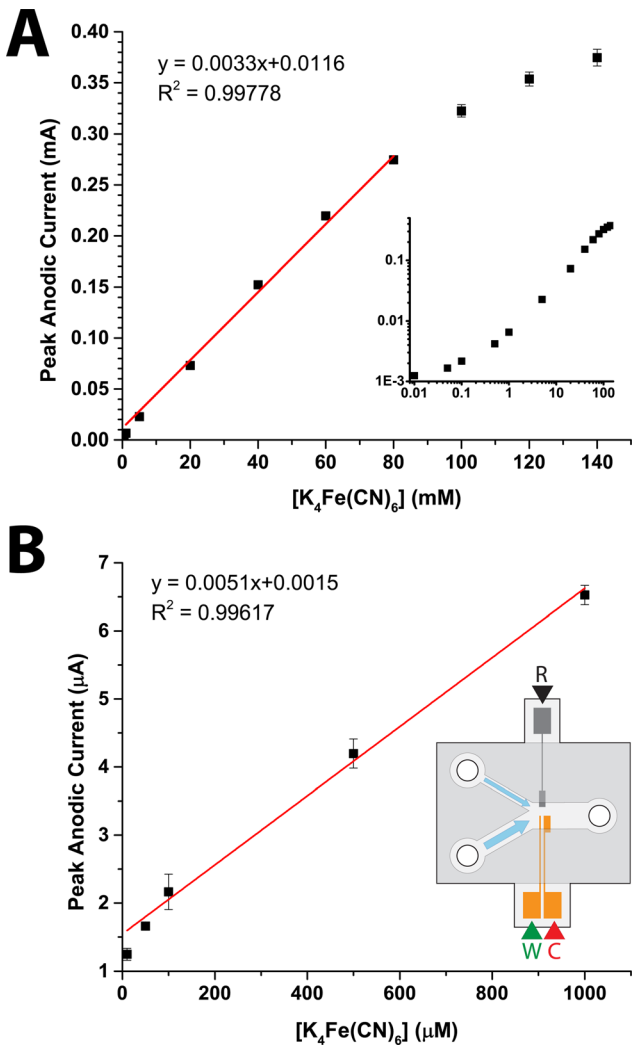

FIG. 5. On-chip electrochemical sensing with structured electrodes. Chronoamperometry was used to measure the anodic current produced by different concentrations of potassium ferricyanide. Two distinct linear ranges were observed: (a) 1–100 mM and (b) 1–1000 μM. Insets: full range of calibration curve and schematic of sensing microfluidic device. Error bars represent the standard deviation of the multiple runs made for each data point with the same device.

IV. CONCLUSIONS

This work presents a novel simple, rapid, and cost-efficient bench-top approach for the integration of high surface area 3D structured electrodes into polystyrene-poly(dimethylsiloxane) microfluidic devices. The use of xurography of adhesive films enables the quick prototyping of both the structured electrode and microfluidic layers. For the assembly of complete microfluidic devices that encapsulate the structured electrodes, the optimized PS-PDMS bonding protocol results in strong bonds capable of resisting delamination under gaseous pressure up to ~150 kPa and fluid flow rates up to ~5.5 ml/min. In addition, the fabrication and bonding procedures did not adversely impact the electrochemical performance of the 3D structured electrodes, as shown through cyclic voltammetry measurements of their electro-active surface area. Finally, the on-chip electrochemical sensing capabilities of the bench-top fabricated microfluidic devices were demonstrated through sensing of a model redox compound, where the 3D structured electrodes exhibited excellent linearity over 5 orders of magnitude and ultra-high sensitivity per surface area. The bench-top fabrication approach presented in this work could aid in the prototyping and development of inexpensive point-of-care devices for sensing and diagnosis.

ACKNOWLEDGMENTS

This work was supported through the Natural Sciences and Engineering Research Council (RGPIN/418326) and a Canada Foundation for Innovation Leaders Opportunity Fund. J.M.M. is the recipient of an Early Researcher Award through the Ontario Ministry of Research and Innovation.

[1]B. S. Ferguson, S. F. Buchsbaum, J. S. Swensen, K. Hsieh, X. Lou, and H. T. Soh, Anal. Chem. **81**, 6503 (2009).
[2]F. Liu, A. N. Nordin, F. Li, and I. Voiculescu, Lab Chip **14**, 1270 (2014).
[3]E. V. Dydek, M. V. Petersen, D. G. Nocera, and K. F. Jensen, Lab Chip **12**, 1431 (2012).
[4]H. Sharma, D. Nguyen, A. Chen, V. Lew, and M. Khine, Ann. Biomed. Eng. **39**, 1313 (2010).
[5]M. D. Huntington and T. W. Odom, Small **7**, 3144 (2011).
[6]D. A. Bartholomeusz, R. W. Boutte, and J. D. Andrade, J. Microelectromech. Syst. **14**, 1364 (2005).
[7]J. Greer, S. O. Sundberg, C. T. Wittwer, and B. K. Gale, J. Micromech. Microeng. **17**, 2407 (2007).
[8]M. J. Hancock, F. Yanagawa, Y.-H. Jang, J. He, N. N. Kachouie, H. Kaji, and A. Khademhosseini, Small **8**, 393 (2011).
[9]A. Grimes, D. N. Breslauer, M. Long, J. Pegan, and L. P. Lee, Lab Chip **8**, 170 (2008).
[10]M. Abdelgawad, M. W. L. Watson, E. W. K. Young, J. M. Mudrik, M. D. Ungrin, and A. R. Wheeler, Lab Chip **8**, 1379 (2008).
[11]P. K. Yuen and M. E. DeRosa, Lab Chip **11**, 3249 (2011).
[12]A. Paguirigan and D. J. Beebe, Lab Chip **6**, 407 (2006).
[13]P. J. Kitson, M. H. Rosnes, V. Sans, V. Dragone, and L. Cronin, Lab Chip **12**, 3267 (2012).
[14]D. J. Lipomi, R. V. Martinez, L. Cademartiri, and G. M. Whitesides, *Soft Lithographic Approaches to Nanofabrication* (Elsevier B.V., 2012), pp. 211–231.
[15]C. M. Gabardo, Y. Zhu, L. Soleymani, and J. M. Moran-Mirabal, Adv. Funct. Mater. **23**, 3030 (2013).
[16]J. I. Luna, J. Ciriza, M. E. Garcia-Ojeda, M. Kong, A. Herren, D. K. Lieu, R. A. Li, C. C. Fowlkes, M. Khine, and K. E. McCloskey, Tissue Eng. Part C **17**, 579 (2011).
[17]A. Chen, D. K. Lieu, L. Freschauf, V. Lew, H. Sharma, J. Wang, D. Nguyen, I. Karakikes, R. J. Hajjar, A. Gopinathan, E. Botvinick, C. C. Fowlkes, R. A. Li, and M. Khine, Adv. Mater. **23**, 5785 (2011).
[18]A. N. Sidorov, G. W. Sławiński, A. H. Jayatissa, F. P. Zamborini, and G. U. Sumanasekera, Carbon **50**, 699 (2012).
[19]C. Steuwe, C. F. Kaminski, J. J. Baumberg, and S. Mahajan, Nano Lett. **11**, 5339 (2011).
[20]L. Zhang, X. Lang, A. Hirata, and M. Chen, ACS Nano **5**, 4407 (2011).
[21]J. Yin, J. L. Yagüe, D. Eggenspieler, K. K. Gleason, and M. C. Boyce, Adv. Mater. **24**, 5441 (2012).
[22]D. Taylor, D. Dyer, V. Lew, and M. Khine, Lab Chip **10**, 2472 (2010).
[23]C.-C. Fu, G. Ossato, M. Long, M. A. Digman, A. Gopinathan, L. P. Lee, E. Gratton, and M. Khine, Appl. Phys. Lett. **97**, 203101 (2010).
[24]L. R. Freschauf, J. McLane, H. Sharma, and M. Khine, PLoS One **7**, e40987 (2012).
[25]O. M. Vanderfleet, C. M. Gabardo, F. M. Naeem, J. M. Moran-Mirabal, and L. Soleymani, J. Appl. Polym. Sci. **131**, 40629 (2014).
[26]C.-C. Fu, A. Grimes, M. Long, C. G. L. Ferri, B. D. Rich, S. Ghosh, S. Ghosh, L. P. Lee, A. Gopinathan, and M. Khine, Adv. Mater. **21**, 4472 (2009).
[27]J. D. Pegan, A. Y. Ho, M. Bachman, and M. Khine, Lab Chip **13**, 4205 (2013).
[28]M. A. Eddings, M. A. Johnson, and B. K. Gale, J. Micromech. Microeng. **18**, 067001 (2008).
[29]I. Taurino, S. Carrara, M. Giorcelli, A. Tagliaferro, and G. De Micheli, Surf. Sci. **606**, 156 (2012).
[30]See supplementary material at http://dx.doi.org/10.1063/1.4918596 for two additional figures: Supplementary Figure 1 on the optical characterization of the surface roughness of the structured gold films, and Supplementary Figure 2 on the ability to create simple or complex microfluidic device architectures using the described bench-top fabrication techniques.